

Spatial solitons in periodic nanostructures

A.V. Gorbach and D.V. Skryabin

Centre for Photonics and Photonic Materials, Department of Physics, University of Bath, Bath BA2 7AY, UK

We present the first principle theory of the existence and stability of TE and TM spatial solitons in a subwavelength periodic semiconductor-dielectric structure. We have found that for the wavelength 1550nm and the interface separation close to and less than 100nm the band structure of the linear TE and TM waves becomes similar to the band structure of a homogeneous medium. The properties of TE solitons change accordingly. However, the transverse profiles of the TM solitons continue to reflect the subwavelength geometry of the structure and develop dominant intensity peaks inside the low index dielectric slots. Our stability analysis based on the linearized Maxwell equations indicates that the nonlinear TM waves can be approximated as the evanescently coupled modes of the slot waveguides with the low index dielectric core and the high index semiconductor cladding. Transition to the regime where the slot waveguides start to determine properties of TM waves is associated with the so called Brewster condition.

PACS numbers: 42.65.Tg, 78.67.Pt, 42.70.Nq

I. INTRODUCTION

Recent progress in the fabrication of nanostructures for photonics applications has stimulated research into light trapping and guiding on the subwavelength scale [1, 2, 3]. Surface plasmon polaritons tightly confined to the metal-dielectric interfaces have been at the focus of recent efforts in this direction [4, 5, 6, 7]. The research into plasmons has included studies of their interaction with periodically structured metals, see, e.g. [8], which have been recently extended to soliton structures in periodic arrays of metallic slot waveguides filled with a nonlinear dielectric [9]. The latter work has been a significant and conceptual departure from research into optical solitons in nonlinear waveguides arrays coupled by evanescent waves [10]. The metal dielectric interfaces in [9] are separated by distances much smaller than the wavelength, so that the concept of the coupling induced by the evanescent waves [10, 11] becomes largely irrelevant. New effects can be expected in this regime, which are still waiting to be explored.

Semiconductors also can be used for subwavelength guiding. In particular, silicon photonic wires have been recently promoted as promising and close to practical applications building blocks of photonic chips, where nonlinear and soliton effects have been already extensively researched [12]. The large refractive index of silicon ($n \simeq 3.5$) allows for tight light confinement by the conventional total internal reflection mechanism, giving the simultaneous advantages of strong ultrafast Kerr nonlinearity ($n_2 \simeq 4 \times 10^{-18} \text{m}^2/\text{W}$), controlled dispersion and manageable losses. Losses are a particular problem for plasmons, suggesting that their nonlinear functionality is likely to become more viable if gain is introduced into the dielectric [13, 14]. Two photon and free carrier induced absorptions are traditionally thought of as hampering the attractiveness of silicon for nonlinear applications, but these often can be lived with [15, 16] or managed, e.g. by the electrically removing free carriers from the waveguide core [12, 17, 18]. There are also other

highly nonlinear semiconductors and glasses which can be useful for various on-chip applications. In particular, many of the soliton experiments in planar waveguide arrays have been performed using doped GaAs ($n = 3.47$, $n_2 = 3.3 \times 10^{-17} \text{m}^2/\text{W}$) structures [19].

While an isolated silicon or GaAs photonic wire confines light within an area of the order of the wavelength inside the material squared (λ_{vac}^2/n^2), bringing two wires together with a separation of few tens of nanometers produces a strong intensity peak *in-between the wires*, with the field predominantly polarised perpendicular to the interface between the wires (TM-modes). This type of waveguides is called slot waveguides and they provide an elegant method of focusing light into a subwavelength region [20]. One can ask a question about the existence of solitary waves having subwavelength dimensions in arrays of the semiconductor-dielectric slot waveguides. The losses in such arrays are expected to be few dB/cm [21, 22, 23]. Measurements of the transverse profile of the slot mode have been reported in [24], while applications of the silicon slot waveguides have been demonstrated for frequency conversion and wavelength division multiplexing [25], as well as for the design of high Q resonators [23] and sensors based upon them [26].

In this work, we consider an infinite array of semiconductor photonic wires with the wire widths and separations taken well below the wavelength. We assume that the photon energy is below the bandgap and the semiconductor acts essentially as a high index nonlinear dielectric. We present analysis of linear and soliton solutions for both TE and TM polarizations using first principle Maxwell equations. The TE solitons undergo a smooth transformation from the case, which can be well understood in terms of the evanescently coupled waveguides into the solitons of a quasi-homogeneous medium, when the widths of all layers become much less than the wavelength. Conversely and centrally to our work, the TM solitons, under the same change of geometry, evolve into structures with the dominant intensity peaks located outside the semiconductor, i.e. in the low index material.

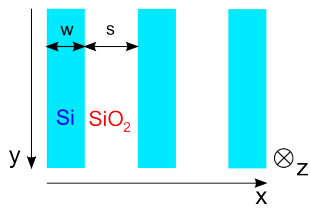


FIG. 1: (Color online) One dimensional periodic structure consisting of layers of high index semiconductor such as silicon (width w) and low-index dielectric such as silica glass (width s).

These peaks become the prevailing features as the separation of high index semiconductor waveguides is reduced. Thus the TM solitons are not transformed into the solitons of the quasi-homogeneous medium, which does not distinguish between polarizations. Our analysis strongly suggests that for subwavelength separations, the TM solitons can be qualitatively considered as discrete solitons composed of the coupled modes of the slot waveguides. We also propose and apply a technique to study linear stability of solitons within the framework of the linearised Maxwell equations.

II. MAXWELL EQUATIONS AND SOLITON EQUATIONS

The array of slot waveguides we consider below is a periodic structure of narrow layers of a high index semiconductor material (material s , e.g., silicon) embedded into a low index dielectric material (material g , e.g., silica glass), see Ref. [21] and Fig. 1. The separations of the semiconductor layers vary from 500 to 50nm, and the width of the layers is between 220 and 95nm. The vacuum wavelength is taken to be $\lambda_{vac} = 1.55\mu\text{m}$. Our analysis is based on the nonlinear Maxwell equations in the 2 dimensional geometry:

$$\vec{\nabla} \times \vec{H} = -ikc\epsilon_0\vec{D}, \quad \vec{\nabla} \times \vec{E} = i\frac{k}{c\epsilon_0}\vec{H}, \quad (1)$$

where $k = 2\pi/\lambda_{vac}$, c is the speed of light in vacuum, ϵ_0 is the vacuum permittivity, and for electric \vec{E} and magnetic \vec{H} fields it is assumed that $\vec{\mathcal{E}}, \vec{\mathcal{H}} = \frac{1}{2}\vec{E}, \vec{H} \cdot \exp(-ikct) + c.c.$ Light propagation is assumed to be along the z -direction and the x -coordinate is perpendicular to the layers, see Fig. 1.

For the TM-polarized modes (such that only H_y, E_x and E_z are non-zero) the Maxwell equations are reduced to

$$\partial_{zz}E_x - \partial_{zx}E_z = -k^2D_x, \quad (2)$$

$$\partial_{zx}E_x - \partial_{xx}E_z = k^2D_z, \quad (3)$$

$$\partial_zH_y = ikc\epsilon_0D_x. \quad (4)$$

While for the TE-polarized modes, only E_y, H_x and H_z

are non-zero and the resulting equations are

$$\partial_{zz}E_y = -k^2D_y, \quad (5)$$

$$\frac{k}{c\epsilon_0}H_x = i\partial_zE_y, \quad \frac{k}{c\epsilon_0}H_z = -i\partial_xE_y. \quad (6)$$

We only need to solve these equations for the electric field components in both the TE and TM cases. The constitutive relation is taken as for isotropic materials

$$\vec{D} = \epsilon\vec{E} + \frac{1}{2}\chi_3[|\vec{E}|^2\vec{E} + \frac{1}{2}(\vec{E} \cdot \vec{E})\vec{E}^*], \quad (7)$$

where \vec{D} is the displacement in SI units normalized to ϵ_0 . The above expression for \vec{D} is an approximation for anisotropic semiconductors, but its use is sufficient to demonstrate the reality of the effects we are interested in and helps to improve the transparency of our results and to simplify the complex numerical calculations. We also neglect linear and nonlinear absorptions, which influence, but do not prevent observation of soliton effects [15, 16].

In our numerical approach, we do not force boundary conditions at the interfaces, but instead assume that the linear permittivity ϵ and the nonlinear susceptibility χ_3 change continuously (but sharply) between their respective values for the material s (silicon) and material g (silica glass). We model the structure by taking

$$\epsilon(x) = \epsilon_g + \sum_j (\epsilon_s - \epsilon_g)K_j(x), \quad (8)$$

where $K_j(x) = \exp\{-[(x - x_j)/w]^{10}\}$ is the array of super-gaussian functions, $j = 0, \pm 1, \pm 2 \dots$, $x_j = j(s+w)$ is the position of the j th semiconductor layer, w is its width and s is the side to side separation of the semiconductor layers (see Fig. 1), $\epsilon = n^2$ and $n_g = 1.44$, $n_s = 3.48$. χ_3 is linked to the n_2 coefficient (measured in m^2/W) and found in the tables as $\chi_3 = \frac{4}{3}n_2\epsilon_0c$ [27]. Thus it is convenient to introduce the function

$$\gamma(x) = \epsilon_0cn_2(x)\epsilon(x), \quad (9)$$

where

$$n_2(x) = n_{2,g} + \sum_j (n_{2,s} - n_{2,g})K_j(x), \quad (10)$$

$$n_{2,g} = 2.5 \cdot 10^{-20} \text{m}^2/\text{W}, \quad n_{2,s} = 4 \cdot 10^{-18} \text{m}^2/\text{W}.$$

A. Equations for TM solitons

We seek soliton solutions of Eqs. (2), (3), (7) in the form

$$E_x = f(x)e^{iqkz}, \quad E_z = ig(x)e^{iqkz}. \quad (11)$$

After some algebra, we find that the real functions f and g obey the system of the first order ordinary differential

equations

$$f' = \frac{k\partial F/\partial g - q[\epsilon' + \gamma'(f^2 + g^2/3)]f}{q\{\epsilon + \gamma[3f^2 + g^2/3]\}}, \quad (12)$$

$$g' = -\frac{k\partial F/\partial f}{q\{\epsilon + \gamma[3f^2 + g^2/3]\}}, \quad (13)$$

where prime indicates first derivative in x and the parameter q measures the relative change of the propagation constant with respect to its vacuum value k . The function $F(f, g)$ is given by

$$F = \frac{\gamma^2 f^6}{2} + \frac{\gamma[4\epsilon - 3q^2]f^4}{4} + \frac{\epsilon[\epsilon - q^2]f^2}{2} + \frac{\gamma q^2 g^4}{4} + \frac{q^2 \epsilon g^2}{2} + \frac{\gamma f^2 g^2}{3} \left[\gamma \left(f^2 + \frac{g^2}{6} \right) + \epsilon - \frac{q^2}{2} \right]. \quad (14)$$

F becomes the first integral of Eqs. (12)-(13) in the case of a homogeneous medium (when ϵ and γ are x independent) [28].

B. Equation for TE solitons

Soliton solutions of Eqs. (5), (7) are sought in the form

$$E_y = u(x)e^{iqkz}, \quad (15)$$

which results in the familiar stationary nonlinear Schrödinger equation (NLSE)

$$u'' + k^2(\epsilon - q^2)u + k^2\gamma u^3 = 0. \quad (16)$$

In a case of the evanescently coupled semiconductor waveguides, the above equation is readily transformed into a set of coupled mode algebraic equations, giving familiar discrete soliton solutions [10]. In the limit when w and s are much less than λ_{vac} , one should expect the soliton profiles to be close to the ones known from the NLSE with constant coefficients. Such qualitative conclusions are, however, difficult to make simply by looking at the equations for TM solitons. A useful insight into the difference between the TM and TE waves can be obtained when considering linear modes of the structure.

III. LINEAR MODES, BAND STRUCTURE AND BREWSTER CONDITION

For $\gamma \equiv 0$ Eqs. (12)-(14) for TM waves are reduced to the linear eigenvalue problem

$$q^2 k^2 f = \left(f'' + \frac{\epsilon'}{\epsilon} f' \right) + \left[k^2 \epsilon + \frac{\epsilon''}{\epsilon} - \left(\frac{\epsilon'}{\epsilon} \right)^2 \right] f. \quad (17)$$

It can be seen that the sharp jumps in ϵ can be compensated only if the function f itself changes sharply. The jump in f is determined by the refractive index contrast, and follows from the continuity of D_x at an interface.

For TE waves the linear equation is

$$k^2 q^2 u = u'' + k^2 \epsilon u. \quad (18)$$

Therefore, jumps in ϵ only force the second derivative of u to change accordingly, while u itself stays smooth.

According to the Floquet-Bloch theorem, linear modes for TE and TM cases (f or u) can be represented in the form $r(x)\exp(ik_B kx)$, where $r(x+w+s) = r(x)$ and $w+s$ is the period. All eigenvalues $q^2 > 0$ are parameterized by the Bloch wavenumber k_B , $0 \leq |k_B| \leq \pi/(k(w+s))$. In the linear case, the problem is tractable analytically with exact boundary conditions at the interfaces [29, 30]. The discussions in [29, 30] are focused on the band structure and miss important for us features of the linear mode profiles, which are highlighted below.

If we choose $w = 220\text{nm}$ and a sufficiently large separation between the semiconductor layers $s = 500\text{nm}$, then the spectrum $q^2(k_B)$ for both TE and TM modes has two bands, see Figs. 2(a) and (b). The $k_B = 0$ and $k_B = \pi/(k(w+s))$ Bloch modes of the top band consist, respectively, of the in-phase and out-of-phase modes of the individual waveguides, see insets in Figs. 2(a) and (b). The TE Bloch modes can be well approximated using the well known tight-binding approach [10], when the Bloch mode is represented by a superposition of the modes of the individual semiconductor layers. For TM modes, the field structure is dominated by jumps at the boundaries. However, the field overlap in the dielectric (silica) layers still happens via exponentially decaying tails, and so the tight binding approximation is justifiable here as well. In both cases, the tight binding model will readily reproduce the almost sinusoidal profile of $q^2(k_B)$ for the top band. The modes of the top band with small k_B experience normal (as in free space) diffraction, while those with k_B near π have anomalous diffraction. This is in contrast to the system of coupled metallic slot waveguides, where the situation is the opposite due to ϵ being negative in metals [9].

As we reduce s , whilst keeping $w = 220\text{nm}$, we find that for TM modes, the gap below the top band shrinks and disappears at the Brillouin zone edges. The gap closure happens when $s = (\pi\sqrt{\epsilon_s + \epsilon_g} - \epsilon_s k w)/\epsilon_g/k \equiv s_0$. This result is derived using the exact boundary conditions at the interfaces and is reproduced well while numerically solving Eq. (17) ($s_0 \approx 125\text{nm}$ for $w = 220\text{nm}$). The critical value s_0 exists due to the Brewster angle condition, which gives zero reflection of the TM polarized wave from an interface. When the Brewster condition is satisfied, then the resonant Bragg scattering is canceled, the gap is closed and the periodic medium becomes transparent [29, 30]. For $s < s_0$ the gap in q opens again, while the lower band continues to sink and soon disappears below the $q^2 = 0$ line. The band structures of TM waves and Bloch modes in this regime are shown in Fig. 2(d).

Crucially, at the instant when $s < s_0$ the geometry of the top band TM modes undergoes structural transformation. Specifically, the out-of-phase modes at the

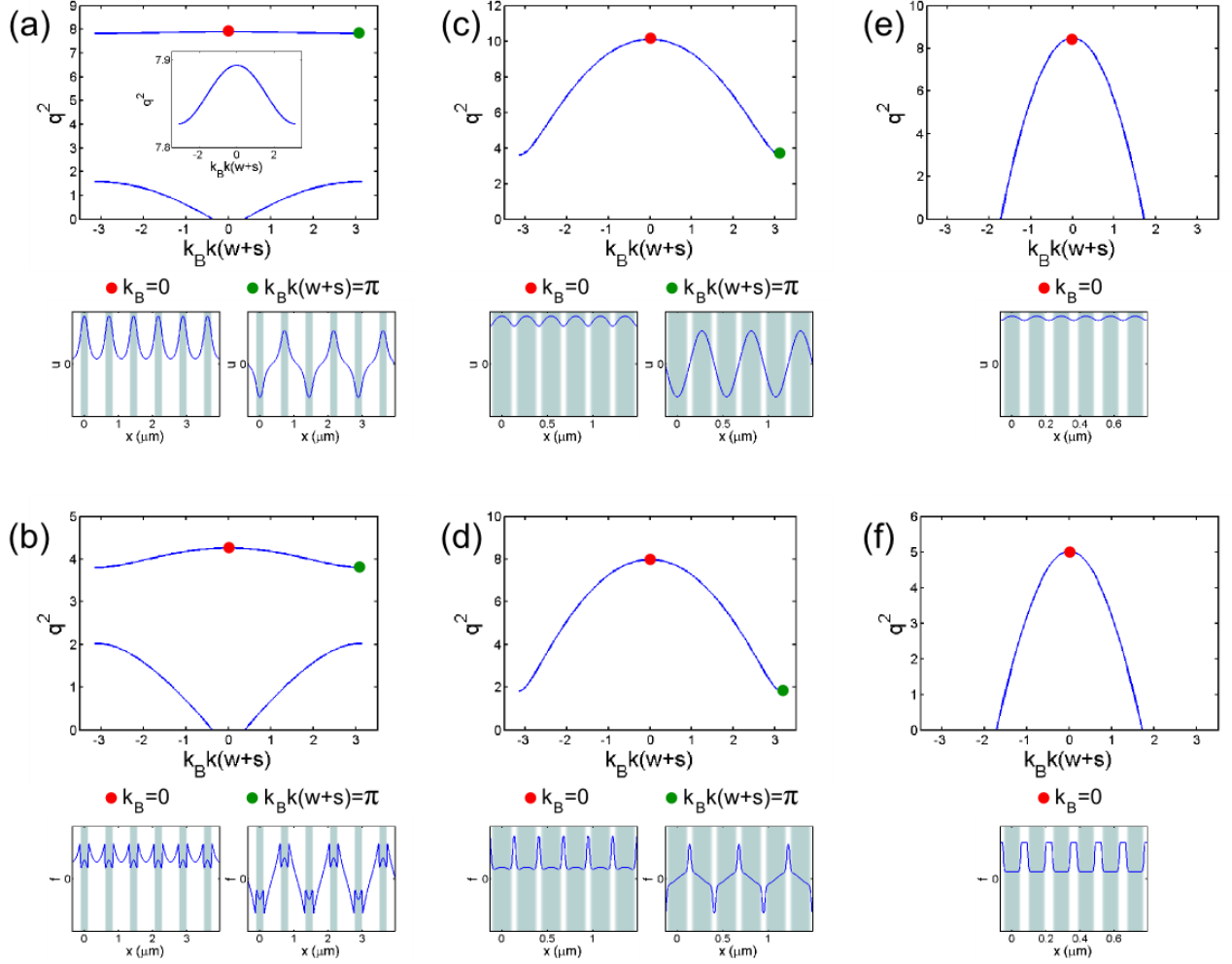


FIG. 2: (Color online) Spectra of linear TE (a,c,e) and TM (b,d,f) waves in different periodic structures: (a),(b) $w = 220\text{nm}$, $s = 500\text{nm}$; (c),(d) $w = 220\text{nm}$, $s = 50\text{nm}$; (e), (f) $w = 95\text{nm}$, $s = 50\text{nm}$. Small plots show the mode profiles at the centre and edge of the Brillouin zone from the top band. The inset in (a) shows zoom of the top band.

bottom of the band now cross zero not inside the low index material, but inside the high index one, cf. insets in Fig. 2(b) and (d). This transformation signals a qualitative transition to the regime, where it is appropriate to consider our periodic medium as an array of coupled slot waveguides with sub-wavelength light localization inside the low index slots. Indeed, the field intensity of the TM modes at the top of the band now peaks in-between the semiconductor layers and is strongly depressed inside them, see inset in Fig. 2(b).

In contrast to the TM modes, the first band gap of the TE modes never shrinks to zero, and the structural transformation of the profiles of the top-band TE modes does not happen, cf. Figs. 2(a) and (c). The lower band of the TE spectrum sinks below the $q^2 = 0$ line in a way similar to the TM case.

Further reduction of either s or w (or both of them simultaneously) leads to the edges of the transmission band sinking below the $q^2 = 0$ cutoff for both the TE and TM

modes, so that the out-of-phase modes corresponding to anomalous diffraction gradually disappear, see Figs. 2(e) and (f). The linear spectrum in this regime qualitatively reproduces that of a homogeneous medium, so that the description of the structure with an effective index approach becomes relevant. The TE modes in this regime approach the ones of a homogeneous medium. E.g., the TE mode in the middle of the Brillouin zone tends to a constant, see inset in Fig. 2(e). At the same time the TM modes remain deeply modulated, with pronounced jumps at interfaces, see inset in Fig. 2(f).

The excitation of a periodic medium with a narrow beam naturally results in a diffractive spreading. We can estimate the diffraction length l_d of a beam with a radius d as $l_d = kd^2/|\delta|$, where the diffraction coefficient

$$\delta = \frac{d^2 q}{dk_B^2}. \quad (19)$$

Provided the initial excitation has a flat phase across the

beam, the δ is calculated at $k_B = 0$ of the highest band. For $s = 50\text{nm}$ and $w = 220\text{nm}$ or $w = 95\text{nm}$ the diffraction length of the 500nm wide beam is approximately $3\mu\text{m}$ and is roughly the same for TE and TM waves. However, for $w = 500\text{nm}$ the l_d for TM modes is still around $3\mu\text{m}$, while for TE modes it is about an order of magnitude more. We note that the overlap of the TE modes through the evanescent fields inside the dielectric layers is smaller than the overlap of the TM modes. This is consistent with the difference of the diffraction lengths.

Using the soliton concept we aim to demonstrate that preventing this fast spreading and achieving subwavelength localisation of light is possible. Below we are establishing existence and study stability of solitons and, on this basis, are making some assumptions about their mobility. The propagation studies, which will allow full exploitation of soliton dynamics and functionality, require development of a different set of numerical tools and are postponed for the future.

IV. NUMERICAL METHODS FOR FINDING SOLITON SOLUTIONS AND DETERMINING THEIR STABILITY

Soliton solutions of Eqs. (12)-(14) discussed in the next chapter have been found using the shooting method with zero boundary conditions at infinity. Since the nonlinearities of silica and silicon are positive, the soliton propagation constant q has to be greater than the one for the linear waves, i.e. $q > q_{lin}$. Here q_{lin} is the propagation constant of the $k_B = 0$ linear mode of the top band.

To characterize soliton solutions we use the power density P_z defined as the x integrated z component of the time averaged Poynting vector $\langle \vec{S} \rangle$,

$$P_z = \int_{-\infty}^{\infty} \langle S_z \rangle dx, \quad \vec{S} = \vec{\mathcal{E}} \times \vec{\mathcal{H}}, \quad (20)$$

where $\langle \dots \rangle$ denotes time averaging. We plot P_z as the function of the nonlinear phase shift induced by a soliton. The phase shift is defined as the difference between the total and the maximal linear wavenumbers

$$\phi = k(q - q_{lin}). \quad (21)$$

Substituting $\vec{E}(x, z) = (\vec{E}_0(x) + \vec{e}(x, z)) \exp(ikz)$, $\vec{H}(x, z) = (\vec{H}_0(x) + \vec{h}(x, z)) \exp(ikz)$ and linearizing the Maxwell equations for small \vec{e}, \vec{h} we find that the latter obey:

$$i\partial_z \vec{a} = k\hat{A}\vec{a} + \hat{K}\vec{b}, \quad (22)$$

$$k\hat{L}\vec{b} = \hat{M}\vec{a}. \quad (23)$$

Here \vec{E}_0 and \vec{H}_0 are the soliton solutions, $\vec{a} =$

$$[e_x, e_y, h_x, h_y]^T, \quad \vec{b} = [e_z, h_z]^T,$$

$$\hat{A} = \begin{bmatrix} q & 0 & 0 & -1/(c\epsilon_0) \\ 0 & q & 1/(c\epsilon_0) & 0 \\ 0 & c\epsilon_0(\epsilon + \nu_{yy}) & q & 0 \\ -c\epsilon_0(\epsilon + \nu_{xx}) & 0 & 0 & q \end{bmatrix}, \quad (24)$$

$$\hat{K} = \begin{bmatrix} i\partial_x & 0 \\ 0 & 0 \\ 0 & i\partial_x \\ kc\epsilon_0\nu_{xz} & 0 \end{bmatrix}, \quad \hat{M} = \begin{bmatrix} 0 & i\partial_x & 0 & 0 \\ 0 & 0 & 0 & i\partial_x \end{bmatrix}, \quad (25)$$

$$\hat{L} = \begin{bmatrix} 0 & -1/(c\epsilon_0) \\ c\epsilon_0(\epsilon + \nu_{zz}) & 0 \end{bmatrix}, \quad (26)$$

and

$$\nu_{xz} = \frac{2\gamma}{3} [E_{x0}E_{z0}^* + c.c.], \quad (27)$$

$$\nu_{ii} = \frac{2\gamma}{3} [|\vec{E}_0|^2 + 2E_{i0}E_{i0}^*], \quad i = x, y, z \quad (28)$$

By noting that \hat{L} can always be inverted and assuming $\vec{a}(x, z) = \vec{\alpha}(x) \exp(-ik\lambda z)$, we arrive at the eigenvalue problem

$$k^2\lambda\vec{\alpha} = (k^2\hat{A} + \hat{K}\hat{L}^{-1}\hat{M})\vec{\alpha}. \quad (29)$$

We approximate the derivatives in the matrices \hat{K} and \hat{M} by finite differences and are interested in the spatially localized $\vec{\alpha}$ only. Then any λ found with $Im\lambda > 0$ corresponds to an unstable perturbation exponentially growing with the propagation coordinate z .

V. NUMERICAL RESULTS

For TM and TE waves we looked for and found two families of soliton solutions, which differ by the position of their center of symmetry. First, is the family of *on-site solitons*, where the soliton center of symmetry is located in the middle of one of the semiconductor layers. So that, by saying *site* we assume a semiconductor layer. Second is the family of *off-site solitons*, where the soliton center of symmetry is located between the semiconductor layers, i.e. within a slot filled with silica glass.

On-site and off-site soliton profiles for $w = 220\text{nm}$ and $s_0 < s = 500\text{nm}$ are shown in Fig. 3. One can see that for this relatively large separations, the TE and TM solitons have a similar field structure with the light mostly concentrated inside the semiconductor layers. Such field profiles can be well approximated by considering evanescently coupled semiconductor waveguides. The TM soliton is broader for the same power, since the modulus of the corresponding diffraction coefficient is by order of magnitude larger: $\delta_{TM} \simeq -0.32$ and $\delta_{TE} \simeq -0.04$. The

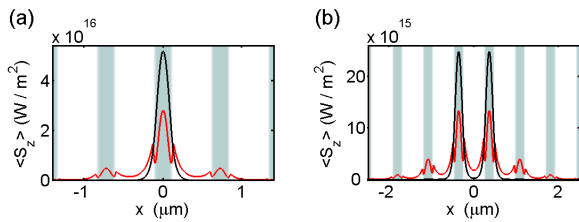


FIG. 3: (Color online) Intensity profiles of TE (black lines) and TM (red/grey lines) solitons: (a) on-site; (b) off-site. The power density for all solitons is fixed to $P_z = 10$ GW/m, see the horizontal lines and markers A and B in Fig. 4. Grayscale background illustrates the underlying periodic structure: $w = 220$ nm, $s = 500$ nm.

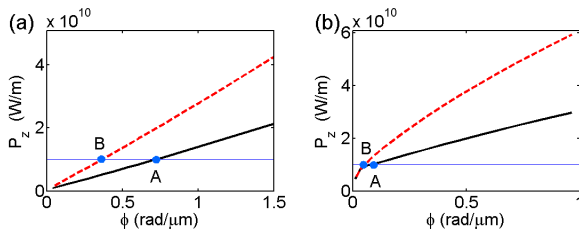


FIG. 4: (Color online) Power density as a function of the phase shift for TE (a) and TM (b) solitons. Black (red/grey) lines correspond to the on-site (off-site) soliton. Solid (dashed) lines indicate stable (unstable) soliton branches. Structure parameters: $w = 220$ nm, $s = 500$ nm. Markers A and B correspond to the on-site and off-site solitons shown in Fig. 3.

on-site solitons are stable in this case, while the off-site ones are unstable. Note, that the on-site and off-site solitons in waveguide arrays described by the discrete nonlinear Schrödinger equation have the same stability property [10, 31]. Power P_z as a function of ϕ is shown in Fig. 4. The on-site and off-site solitons make the same phase shift providing that the latter has a higher power. This is true for both the TE and TM families.

As s approaches and becomes less than s_0 , while w is kept fixed at 220nm, the TM solitons undergo a qualitative change similar to the changes in the linear Bloch modes. The intensity peaks within the slots start to grow and prevail, so that the on-site TM solitons now have a two-peak structure, see Fig. 5(a,c), while the off-site ones have a single dominant peak, see Fig. 5(b,d). Note, that we are still in the regime, when the entire top band of Bloch modes has $q^2 > 0$.

The power P_z as the function of the phase shift ϕ is shown in Figs. 6(a) and (b) for the TE and TM solitons, respectively. For both the TE and TM families, the on-site solitons still give a larger phase shift at a given power than the off-site solitons. The unstable eigenmodes of the off-site solitons from Fig. 5(d) are shown in Fig. 7(a). In both the TE and TM cases, the instability is associated with the anti-symmetric eigenmode (known as "depinning mode" in tight-binding models [31]) and is therefore

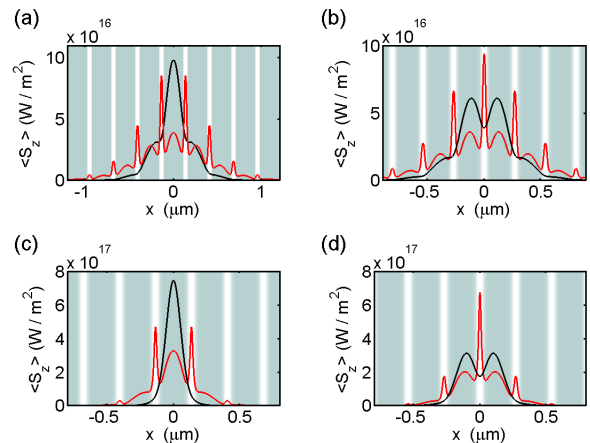


FIG. 5: (Color online) Intensity profiles of TE (black lines) and TM (red/grey lines) solitons: (a,c) on-site; (b,d) off-site: $w = 220$ nm, $s = 50$ nm. The power density for the solitons shown is fixed to: $P_z = 33$ GW/m (a,b) and $P_z = 110$ GW/m (c,d), see the horizontal lines and markers A,B,C,D in Fig. 6.

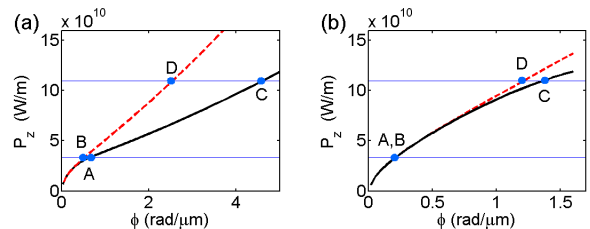


FIG. 6: (Color online) Power density as a function of the phase shift for TE (a) and TM (b) solitons. Black (red/grey) lines correspond to the on-site (off-site) soliton. Solid (dashed) lines indicate stable (unstable) soliton branches. Structure parameters: $w = 220$ nm, $s = 50$ nm. Markers A-D correspond to the on-site and off-site solitons from Fig. 5(a)-(d), respectively.

expected to induce soliton motion across the structure, resulting in emission of dispersive waves and gradual convergence to a stable on-site soliton.

We now reduce the width of the silicon layers to $w = 95$ nm and enter the regime, when the linear diffraction law starts to approach the limit of a homogeneous

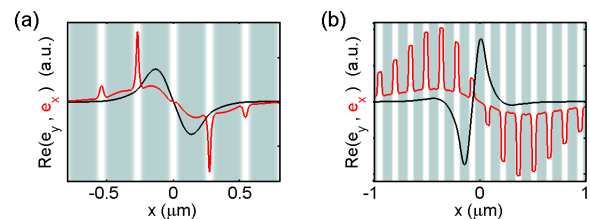


FIG. 7: (Color online) Unstable eigenmodes for TE (black lines) and TM (red/grey lines) solitons: (a) off-site TE and TM solitons from Fig. 5(d); (b) off-site TE soliton from Fig. 8(d) and on-site TM soliton from Fig. 8(c).

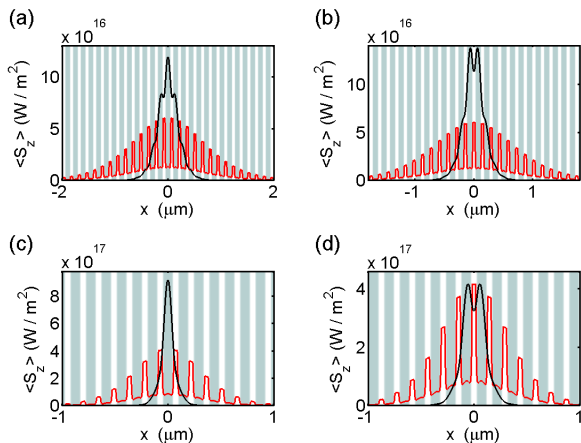


FIG. 8: (Color online) Intensity profiles of TE (black lines) and TM (red/grey lines) solitons: (a,c) on-site; (b,d) off-site: $w = 95\text{nm}$, $s = 50\text{nm}$. Power density for the solitons shown is fixed to: $P_z = 50\text{ GW/m}^2$ (top row) and $P_z = 110\text{ GW/m}^2$ (bottom row), see the horizontal lines and markers A,B,C,D in Fig. 9.

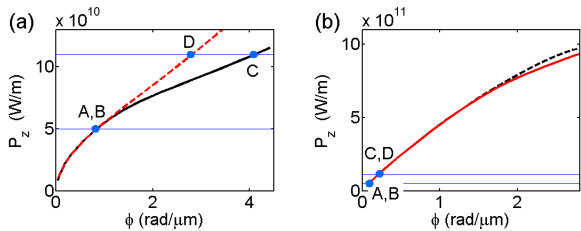


FIG. 9: (Color online) Power density as a function of the phase shift for TE (a) and TM (b) solitons. Black (red/grey) lines correspond to the on-site (off-site) soliton. Solid (dashed) lines indicate stable (unstable) soliton branches. Structure parameters: $w = 95\text{nm}$, $s = 50\text{nm}$. Markers A-D correspond to the on-site and off-site solitons from Fig. 8(a)-(d), respectively.

material (i.e. when the edges of the top band sink below $q^2 = 0$ line and anomalous diffraction regions disappear, see Figs. 2(e),(f)). In this regime, nothing new happens to the TE solitons and their shape feels only very little of the material inhomogeneity, see Fig. 8. At the same time, the structure of the TM solitons is still very inhomogeneous with sharp peaks within silica slots, see Fig. 8. As a significant fraction of light intensity in TM solitons is now concentrated inside slots with low n_2 , TM solitons are noticeably broader than TE solitons at the same level of power, despite the corresponding diffraction coefficient being larger by modulus for TE top band mode: $\delta_{TM} \simeq -0.3$, $\delta_{TE} \simeq -0.4$. Powers as function of ϕ for this geometry are plotted in Fig. 9. While nothing qualitatively changes for TE solitons, on-site and off-site TM solitons exchange their roles: now they produce the same phase shift provided the former has higher power. Importantly, this power exchange is accompanied by the exchange in stability as well. The off-site soliton has

become stable, while the on-site has got the instability with respect to the anti-symmetric linear eigenmode, see Fig. 7(b). This result strongly suggests that the role of an elementary waveguide (or *site*) should be reconsidered for TM solitons in nanostructured periodic medium with the linear spectrum approaching the spectrum of the homogeneous material. Indeed, since both linear and nonlinear modes show strong light confinement inside slots, it is appropriate to consider a slot waveguide as an elementary structure. It means that if the coupled mode approach is to be developed for such geometries in the future, it should use the slot modes as the basis.

We also note that stabilization of the off-site and destabilization of the on-site solitons with respect to the antisymmetric depinning perturbations happens in the discrete nonlinear Schrödinger equation if nonlinear coupling between the adjacent sites is included [32]. Remarkably, in our case the coupling between the slot modes occurs through overlap of the evanescent fields inside the silicon, which is 100 times more nonlinear than the silica glass inside the slots. Similarly to other systems [31, 32], the stability exchange between the on-site and off-site solitons is expected to be accompanied by an enhanced mobility of strongly inhomogeneous TM solitons. The possibility of such enhanced mobility is a problem opened for future investigation, which can reveal new possibilities for all-optical signal steering and manipulation in sub-wavelength structures. We have also checked for the existence of the cross-polarization instabilities, but have not found any for the examples presented above. This issue deserves further more detailed analysis.

VI. SUMMARY

Using the first principle nonlinear Maxwell equations we have developed and applied numerical techniques for finding solitons in periodic semiconductor-dielectric nanostructures and determining their stability.

When the separation between the high index (semiconductor) layers in a periodic structure is reduced beyond the critical value (Brewster condition), the structure of the antisymmetric TM modes at the edges of the highest Brillouin zone undergoes qualitative transformation. Namely the zeros of these modes now appear in the middle of the high index layers and not in the low index ones. This signals transition to the regime when a periodic nanostructure can be considered as an array of coupled slot waveguides for TM waves, rather than an array of coupled high index waveguides guiding by means of total internal reflection. Reducing the interface separation further one enters the regime where the diffraction law in a periodic nanostructure becomes similar to the diffraction in a homogeneous medium. The TE solitons in this quasihomogeneous limit feel little or no periodicity. However, the transverse profiles of the TM solitons reflect the subwavelength periodic structure and have dominant intensity peaks inside the low index

slots. In this regime the TM solitons with the center of symmetry in the middle of a low index slot are stable while the ones centered on a high index layer are unstable. This further facilitates the idea that the TM waves

in periodic nanostructures can be considered as modes of the coupled slot waveguides and calls for developing of the corresponding analytic approaches.

-
- [1] D. J. Sirbully, M. Law, H. Yan, and P. Yang, *J. Phys. Chem. B* **109**, 15190 (2005).
- [2] S. A. Maier, *IEEE J. Selected Topics in Quant. Electronics* **12**, 1214 (2006).
- [3] K. Busch, G. von Freymann, S. Linden, S. Mingaleev, L. Tkeshelashvili, and M. Wegener, *Phys. Reports* **444**, 101 (2007).
- [4] W. L. Barnes, A. Dereux, and T. W. Ebbesen, *Nature* **424**, 824 (2003).
- [5] S. I. Bozhevolnyi, V. S. Volkov, E. Devaux, J.-Y. Laluet, and T. W. Ebbesen, *Nature* **440**, 508 (2006).
- [6] T. W. Ebbesen, C. Genet, and S. I. Bozhevolnyi, *Physics Today* **61**, Issue 5, 44 (2008).
- [7] C. R. Williams, S. R. Andrews, S. A. Maier, A. I. Fernandez-Dominguez, L. Martin-Moreno, and F. J. Garcia-Vidal, *Nature Photonics* **2**, 175 (2008).
- [8] G. Wurtz and A. Zayats, *Laser & Photonics Review* **2**, 125 (2008).
- [9] Y. Liu, G. Bartal, D. A. Genov, and X. Zhang, *Phys. Rev. Lett.* **99**, 153901 (2007).
- [10] F. Lederer, G. I. Stegeman, D. N. Christodoulides, G. Assanto, M. Segev, and Y. Silberberg, *Phys. Reports* **463**, 1 (2008).
- [11] Yu. S. Kivshar, G. P. Agrawal, *Optical Solitons: From Fibers to Photonic Crystals* (Academic Press, 2003).
- [12] R.M. Osgood, Jr., N.C. Panoiu, J.I. Dadap, X. Liu, X. Chen, I.W. Hsieh, E. Dulkeith, W.M.J. Green, and Y.A. Vlasov, *Adv. Opt. Photonics* **1**, 162 (2009); R. Dekker, N. Usechak, M. Först, and A. Driessen, *J. Phys. D* **40**, R249 (2007).
- [13] M. P. Nezhad, K. Tetz, and Y. Fainman, *Opt. Express* **12**, 4072 (2004).
- [14] M. Noginov, V. A. Podolskiy, G. Zhu, M. Mayy, M. Bahoura, J. A. Adegoke, B. A. Ritzo, and K. Reynolds, *Opt. Express* **16**, 1385 (2008).
- [15] W. Ding, C. Benton, A. V. Gorbach, W. J. Wadsworth, J. C. Knight, D. V. Skryabin, M. Gnan, M. Sorrel, and R. M. De La Rue, *Opt. Express* **16**, 3310 (2008).
- [16] C. J. Benton, A. V. Gorbach, and D. V. Skryabin, *Phys. Rev. A* **78**, 033818 (2008).
- [17] R. Jones, H. Rong, A. Liu, A. Fang, M. Paniccia, D. Hak, and O. Cohen, *Opt. Express* **13**, 519 (2005).
- [18] H. Rong, R. Jones, A. Liu, O. Cohen, D. Hak, A. Fang, and M. Paniccia, *Nature* **433**, 725 (2005).
- [19] J. S. Aitchison, D. C. Hutchings, J. U. Kang, G. I. Stegeman, and A. Villeneuve, *IEEE J. Quant. Electron.* **33**, 341 (1977).
- [20] V. R. Almeida, Q. Xu, C. A. Barrios, and M. Lipson, *Opt. Lett.* **29**, 1209 (2004).
- [21] R. Sun, P. Dong, N. Feng, C. Hong, J. Michel, M. Lipson, and L. Kimerling, *Opt. Express* **15**, 17967 (2007).
- [22] T. Baehr-Jones, M. Hochberg, C. Walker, and A. Scherer, *Appl. Phys. Lett.* **86**, 081101 (2005).
- [23] C. A. Barrios, B. Sánchez, K. B. Gylfason, A. Griol, H. Sohlström, M. Holgado, and R. Casquel, *Opt. Express* **15**, 6846 (2007).
- [24] K. Foubert, L. Lalouat, B. Cluzel, E. Picard, D. Peyrade, E. Delamadeleine, F. de Fornel, and E. Hadji, *Appl. Phys. Lett.* **93**, 251103 (2008).
- [25] C. Koos, P. Vorreau, P. Dumon, R. Baets, B. Esembeson, I. Biaggio, T. Michinobu, F. Diederich, W. Freude, and J. Leuthold, *Nature Photonics* **1**, 216 (2009).
- [26] J. T. Robinson, L. Chen, and M. Lipson, *Opt. Express* **16**, 4296 (2008).
- [27] G. P. Agrawal, *Nonlinear Fiber Optics* (Academic Press, 2001), 3rd ed.
- [28] A. Ciattoni, B. Crosignani, P. D. Porto, and A. Yariv, *J. Opt. Soc. Am. B* **22**, 1384 (2005).
- [29] P. Yeh, *Optical Waves in Layered Media* (John Wiley & Sons, 2005).
- [30] J.A. Gaspar-Armenta and F. Villa, *J. Opt. Soc. Am. B* **21**, 405 (2004).
- [31] S. Flach and A. Gorbach, *Phys. Reports* **467**, 1 (2008).
- [32] M. Öster, M. Johansson, and A. Eriksson, *Phys. Rev. E* **67**, 056606 (2003).